

Jingyi Hu and Xingchao Chen

Department of Meteorology and Atmospheric Science, Center for Advanced Data Assimilation and Predictability Techniques  
The Pennsylvania State University, University Park, PA

## 1) Introduction:

- Northwestern South America is one of the rainiest spots on Earth. Rainfall over the region shows a strong diurnal cycle and long-distance offshore propagation, while the physical mechanisms have not been fully understood.
- Past studies hypothesize that diurnal gravity waves induced by heating and cooling of Andes mountains may play an important role (Mapes et al., 2003a, 2003b; Yepes et al., 2020).

## 2) Goal: Examine the long-distance rainfall propagation pattern and identify responsible mechanisms.

## 3) Datasets:

- NASA GPM-IMERG V06 (Huffman et al., 2020) precipitation dataset: March to May, 2001-2020.
- ECMWF ERA5 hourly reanalysis (Hersbach et al., 2020).
- Cloud tracking and classification (Feng et al., 2021; Chen et al., 2022): (1) Mesoscale convective system (MCS); (2) non-MCS deep convection; (3) shallow convection and congestus.

## 4) Diurnal Rainfall Propagation:

- Two local rainfall maxima are observed (Figs. 1a and 2a).
- MCS dominates the rainfall diurnal cycle and propagation (Figs. 1b and 2b).
- Rainfall propagates offshore at 3-10 m s<sup>-1</sup> near Andes (b1 and b2), but much faster at 25 m s<sup>-1</sup> in offshore regions (b3 through b5), producing a long-distance offshore propagation feature over 1200 km (Fig. 2).

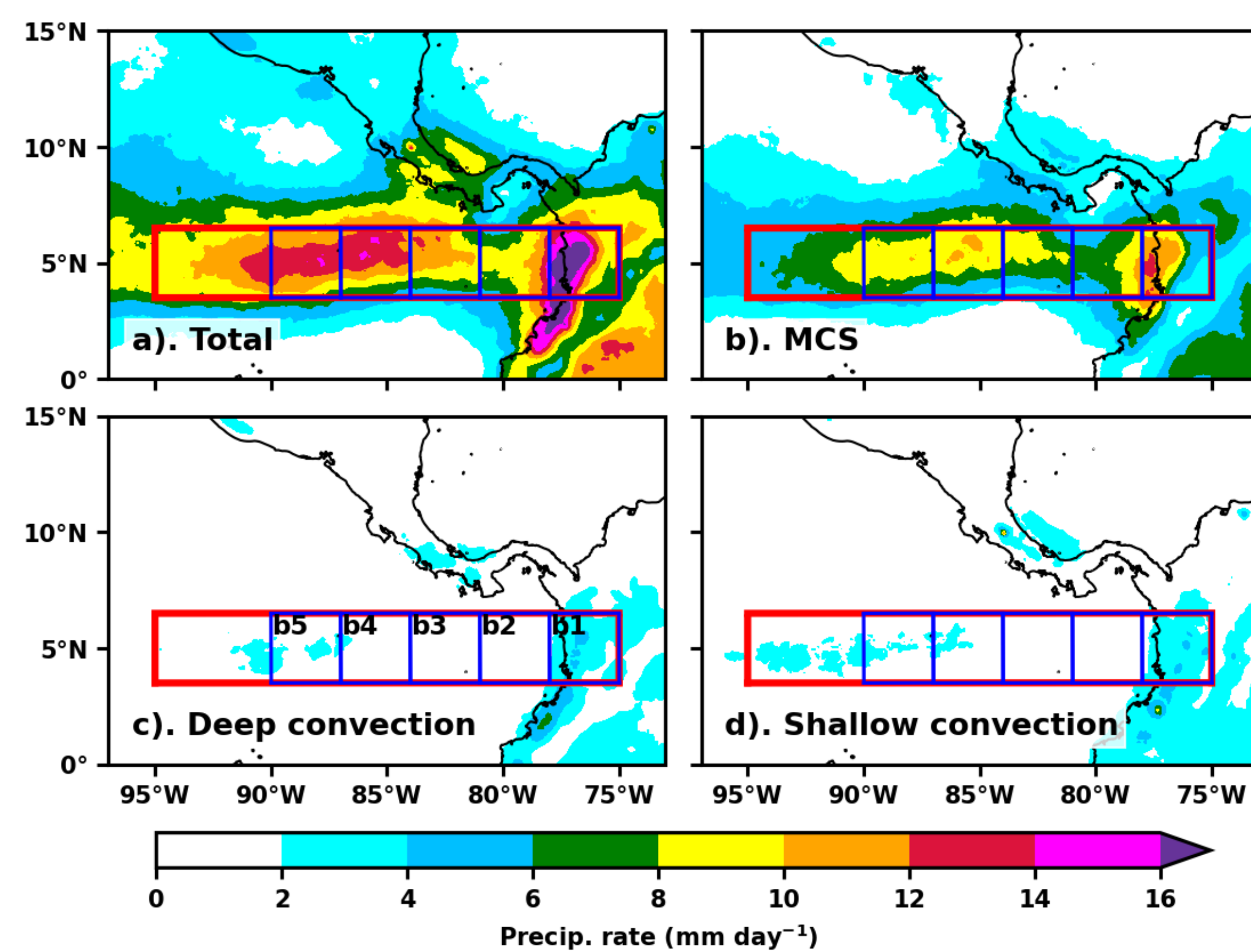


Fig. 1. Spatial diagram of (a) total rainfall and (b)-(d) rainfall from different types of cloud.

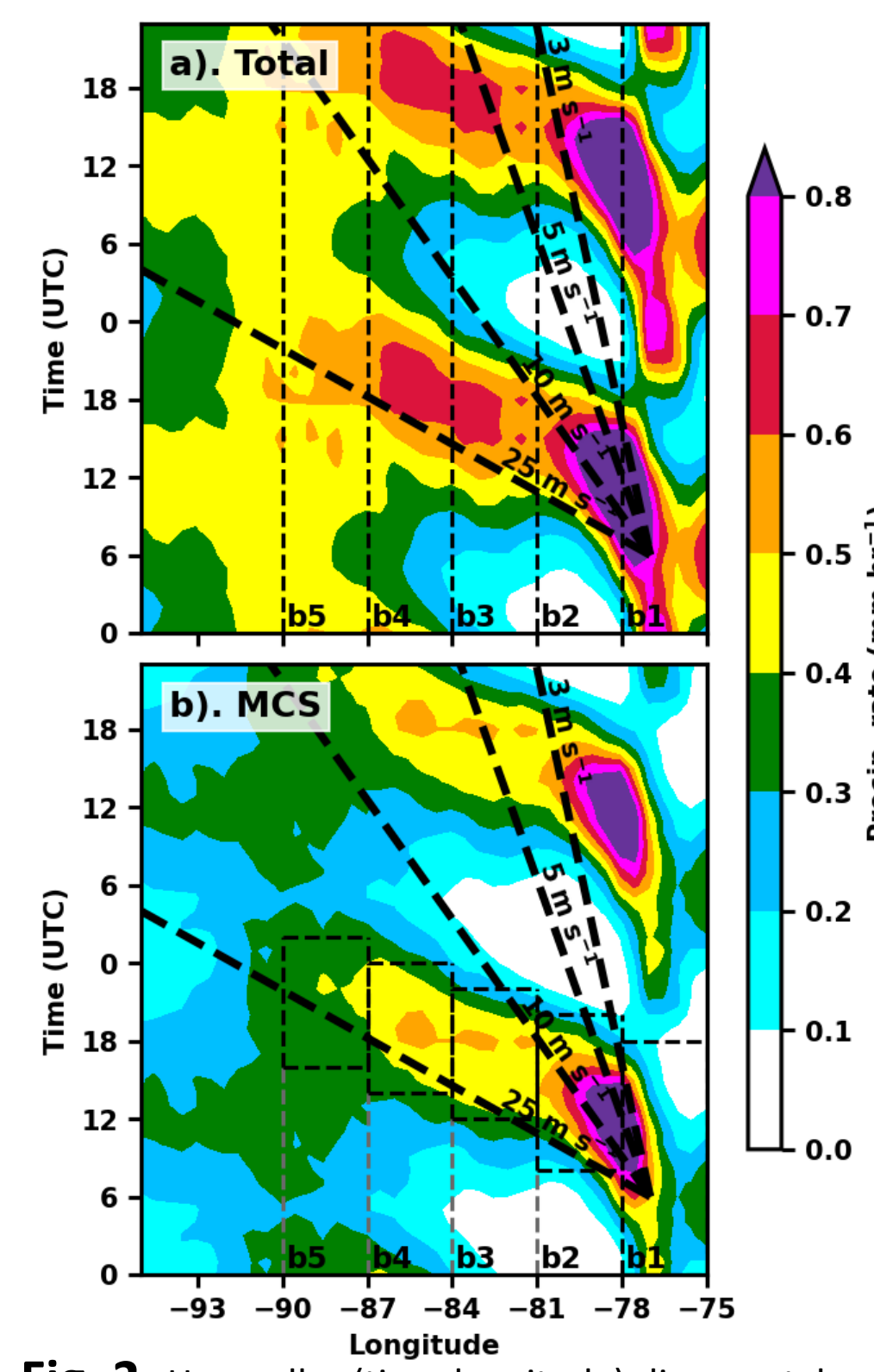


Fig. 2. Hovmöller (time-longitude) diagram taken over the red band in Fig. 1 of (a) total rainfall and (b) rainfall from MCS.

## 5) Rainfall Contribution:

- The observed long-distance rainfall propagation over offshore regions is mainly a result of offshore MCS initiation than MCS propagation from Andes (b3 and b4 in Fig. 3).
- Significant rainfall contribution in offshore regions comes from MCSs initiated offshore during 04-10 UTC (23-05 LT, Fig. 4).

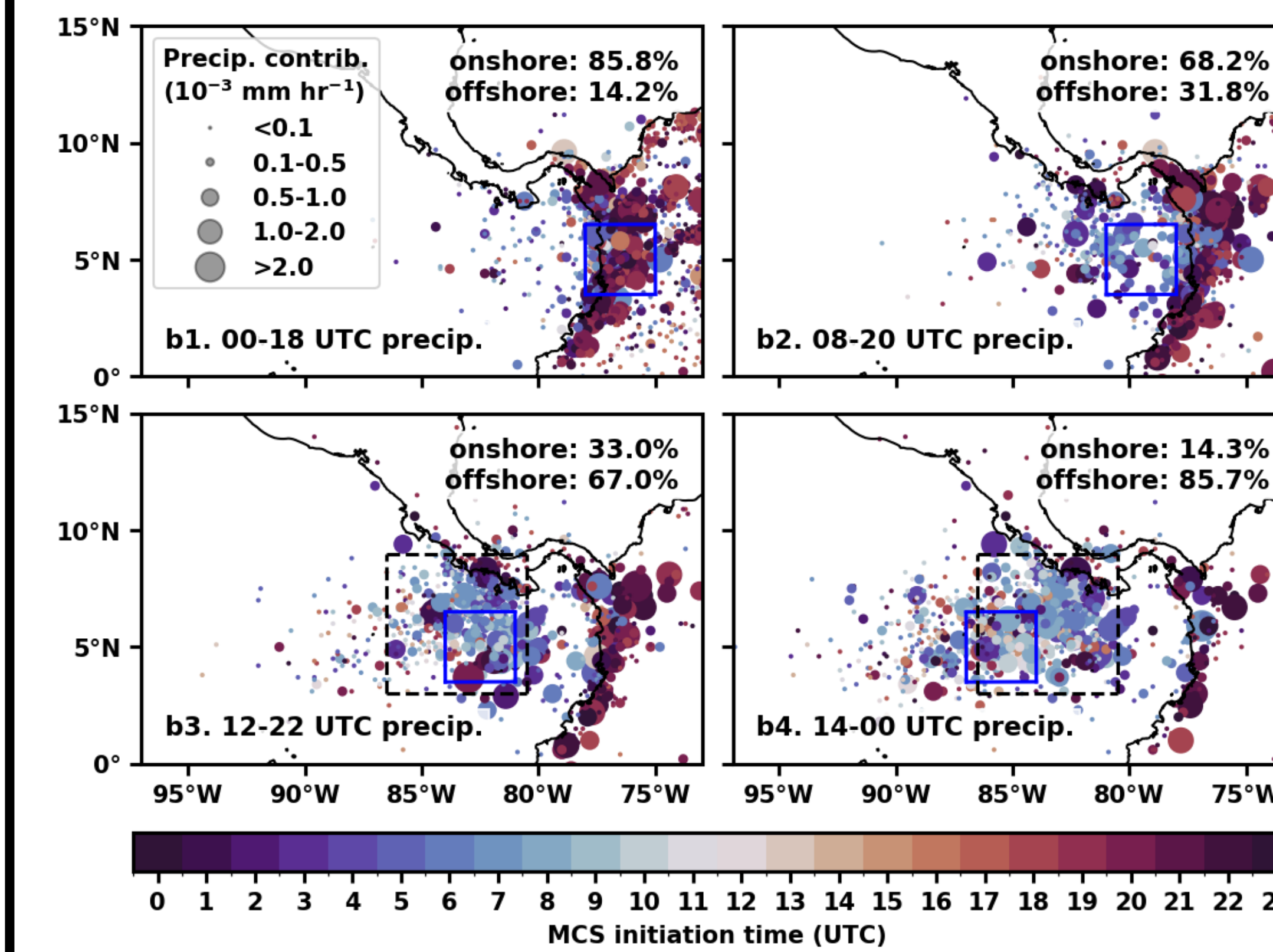


Fig. 3. Spatial diagram of MCS initiation location, time, and rainfall contribution to blue boxes in Fig. 1 with contribution percentage from onshore/offshore MCS.

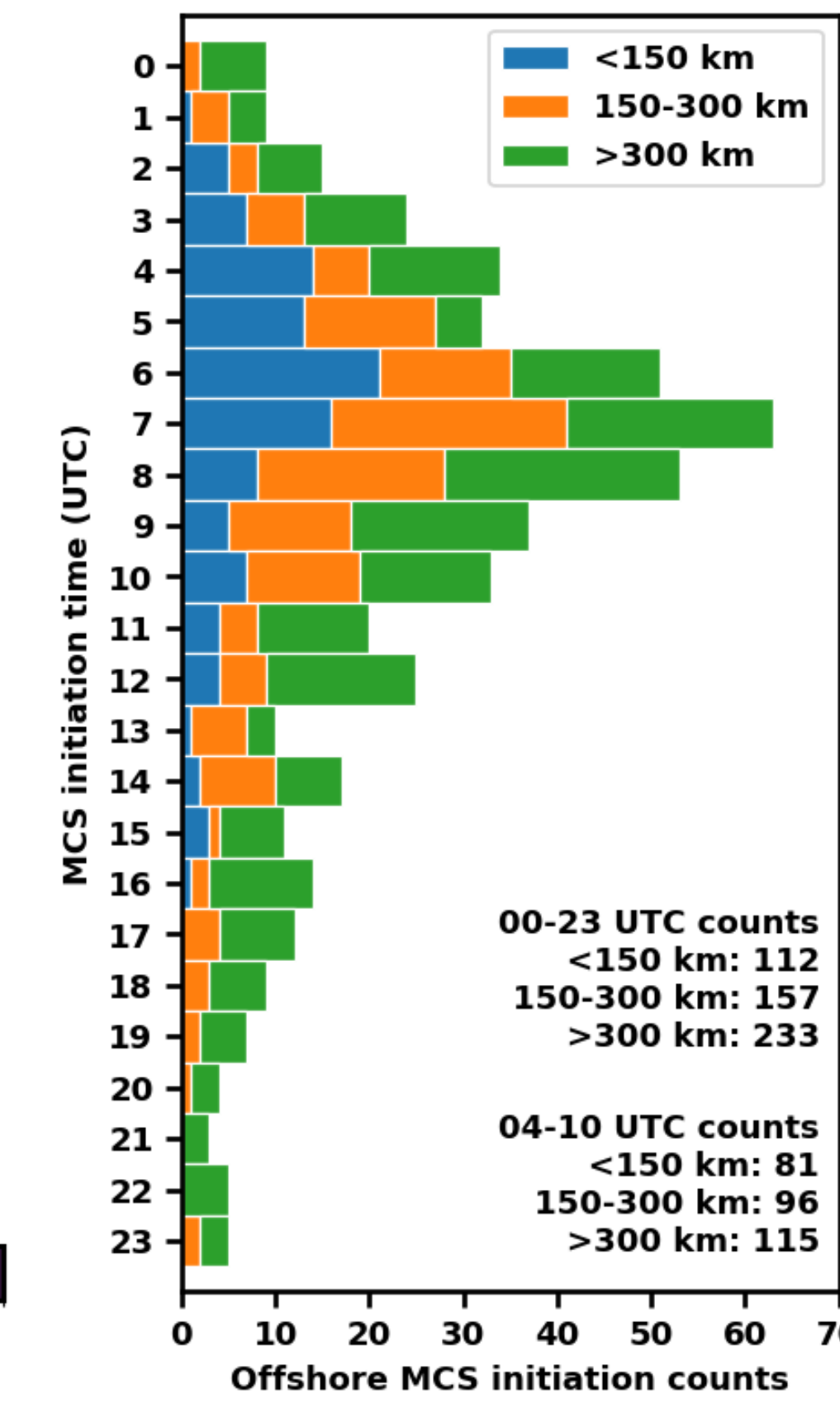


Fig. 4. Statistics of offshore MCS initiation time and counts within the black box in Fig. 3.

## 6) Pre-MCS Local Environment Change:

- Near-coast (<150 km) MCS composite: downward cooling trend from 400 hPa to 700 hPa, but stronger cooling developing from the surface starting from 8 hours pre-initiation (Fig. 6a).
- Open-ocean (>300 km) MCS composite: significant downward cooling trend from 400 hPa to 700 hPa from 5 hours pre-initiation (Fig. 6b).

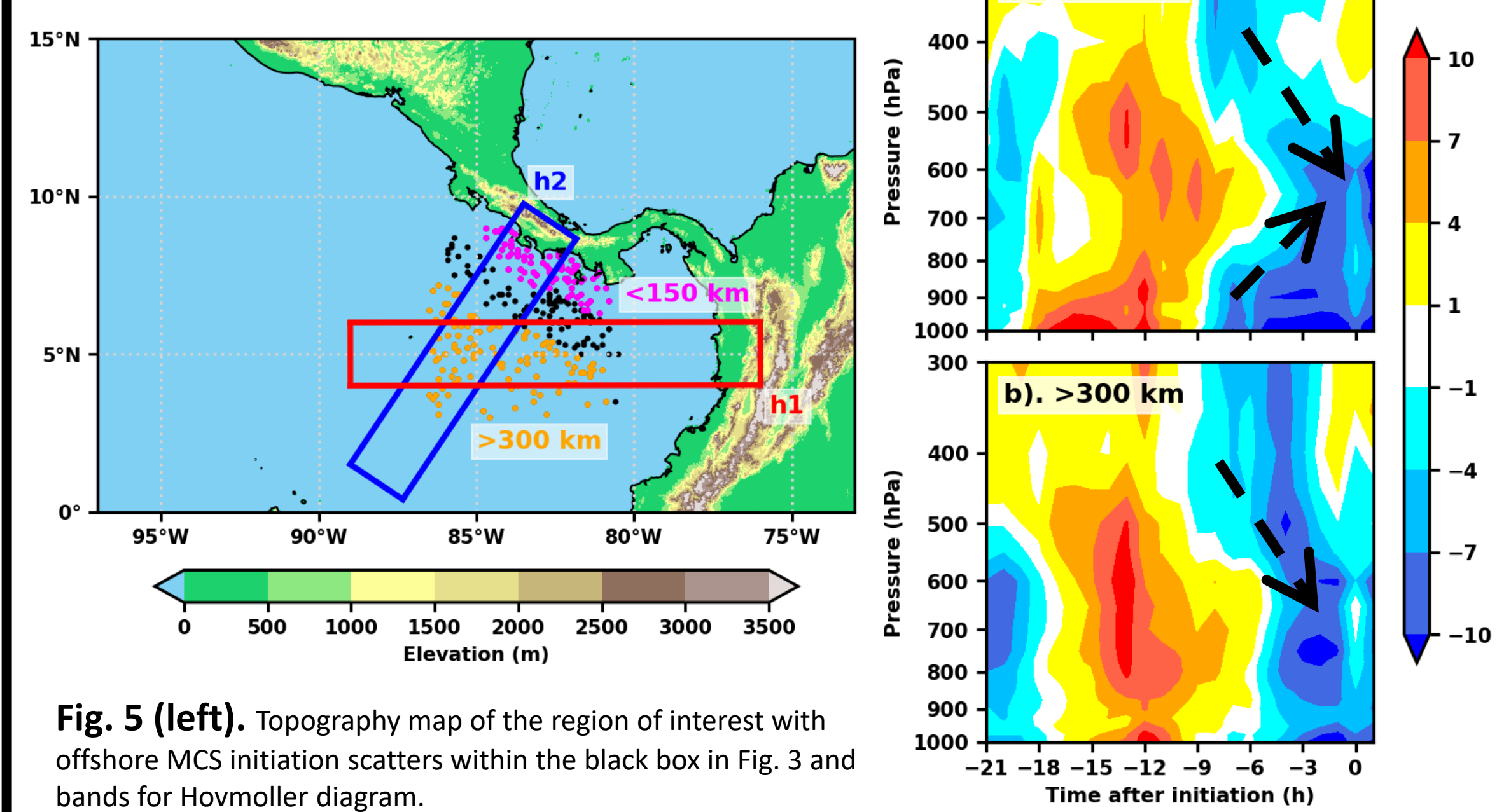


Fig. 5 (left). Topography map of the region of interest with offshore MCS initiation scatters within the black box in Fig. 3 and bands for Hovmöller diagram.

Fig. 6 (right). Composite of potential temperature ( $\theta$ ) tendency prior to MCS initiation for offshore MCSs that initiate (a) within 150km from the nearest coast (magenta scatters in Fig. 5) and (b) over 300km from the nearest coast (orange scatters in Fig. 5).

## 7) Roles of Land Breeze and Gravity waves:

- Near-coast MCS initiations are mainly triggered by land breeze (Figs. 6a and 7).

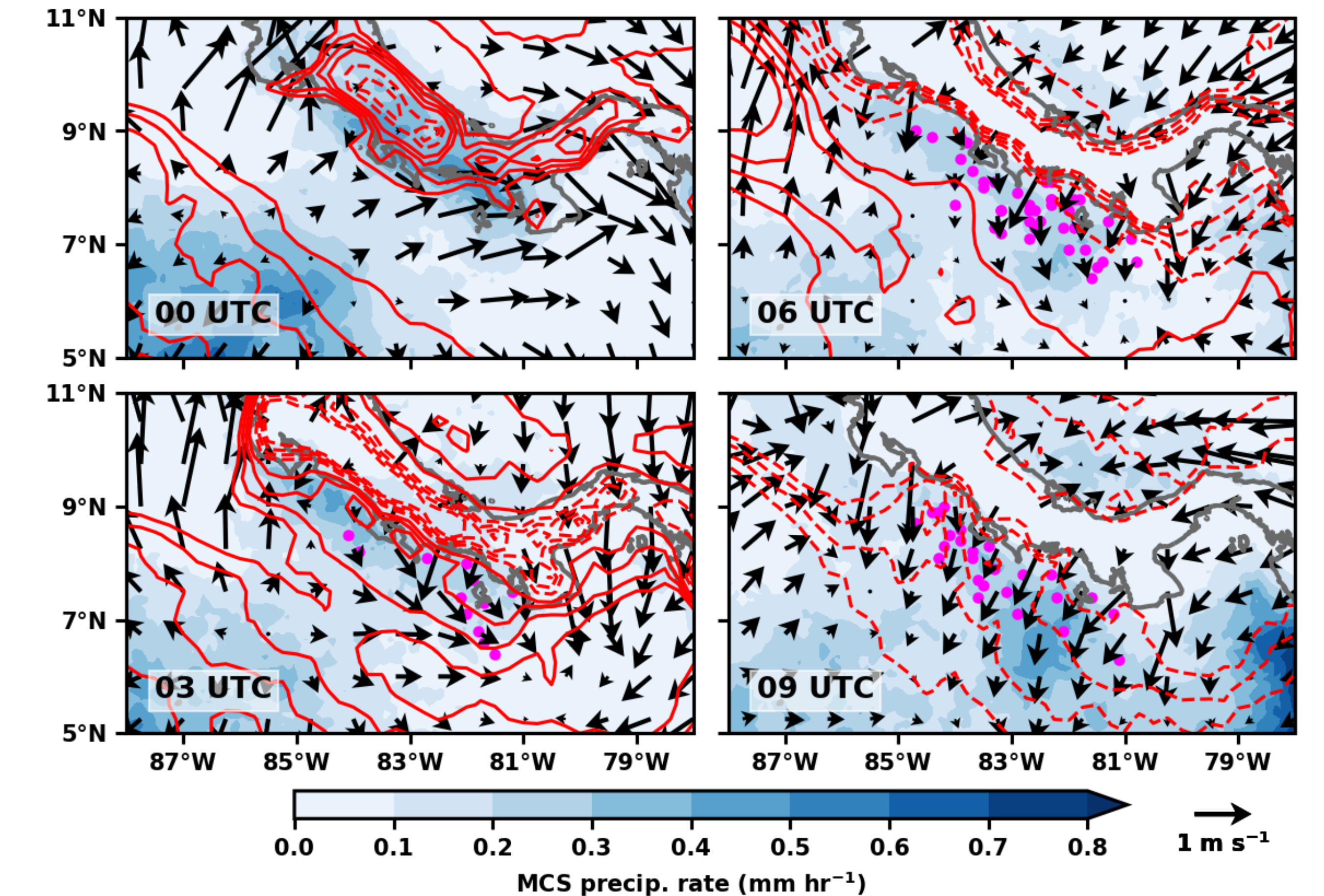


Fig. 7. Spatial diagram of hourly MCS rainfall (filled contour) with 950 hPa diurnal  $\theta$  perturbation (red contours, from -0.4 K to 0.4 K, contour interval 0.1 K, zero contour omitted, and dashed contours negative), diurnal perturbation wind (black arrows), and near-coast MCS initiation location (magenta scatters, as in Fig. 5).

- Open-ocean MCS initiations are mainly triggered by gravity waves (Figs. 6b and 8).
- Two possible sources of gravity waves: Andes (h1 in Fig. 5, Fig. 8a) and Talamanca range (h2 in Fig. 5, Fig. 8b).
- A change in wave amplitude can be identified in their intersection, indicating potential wave interference in open-ocean regions.

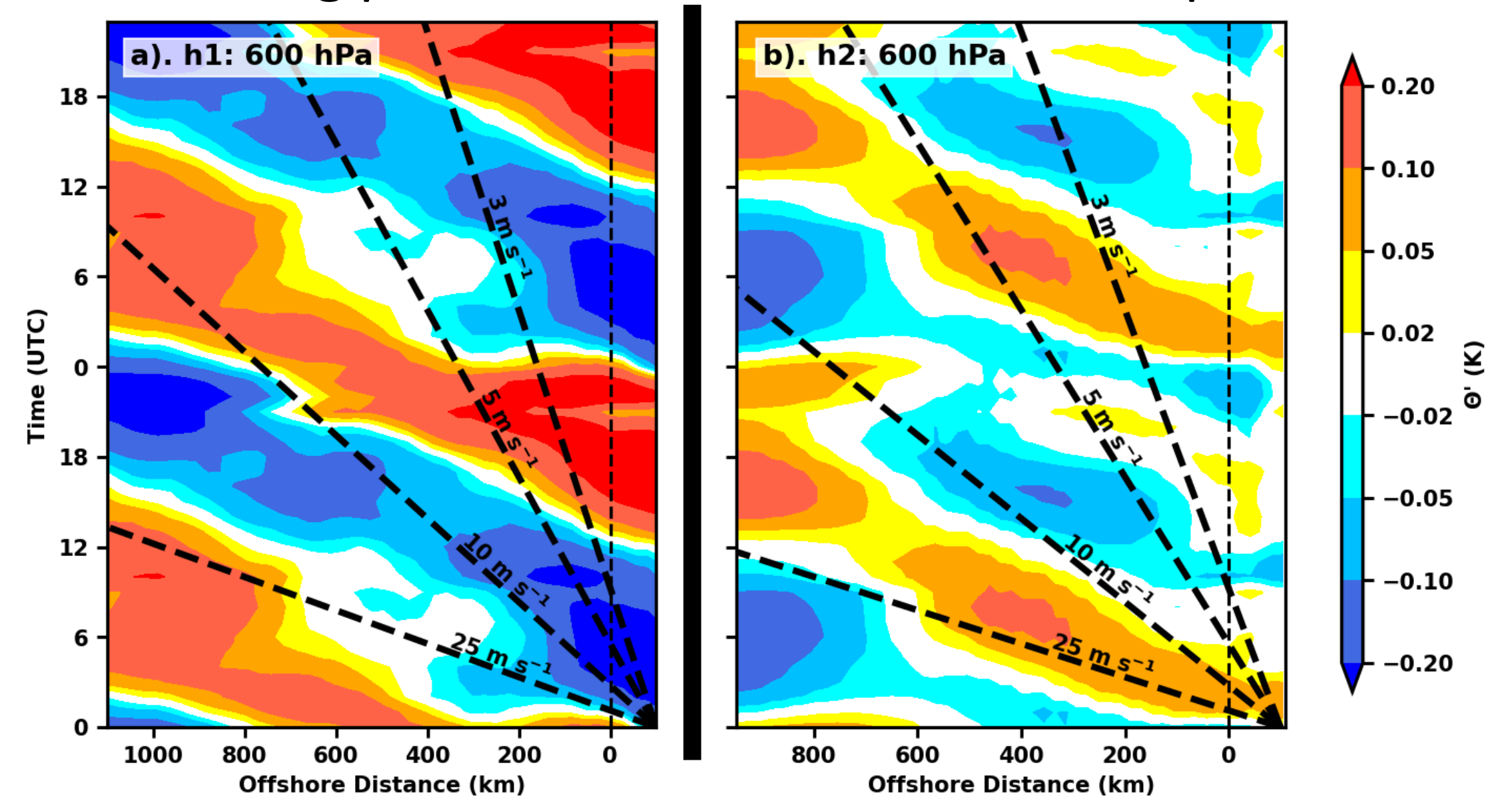


Fig. 8. Hovmöller (time-distance) diagram of diurnal  $\theta$  perturbation taken at 600 hPa filtered by subtracting the mean across the wider dimension from (a) Andes mountains (h1 of Fig. 5) and (b) Talamanca range (h2 of Fig. 5) with reference speed (thick dashed line) and coastline (thin vertical dashed line) designation.

## 8) Conclusion and Future Work:

- Long-distance westward rainfall propagation is dominated by MCS.
- Both MCS initiated from Andes and over ocean contribute to the rainfall propagation.
- Offshore MCS initiation: near-coast initiations are mainly triggered by land breeze, while open-ocean initiations are mainly triggered by the gravity waves from Andes and Talamanca range.
- Further research on MCS initiation triggered by gravity waves will be conducted through numerical modeling.

**Acknowledgement:**  
We would like to thank Zhe Feng from Pacific Northwest National Laboratory (PNNL) for providing the MCS tracking dataset. We also thank Wilbert Weijer from Los Alamos National Laboratory (LANL) and Forrest Hoffman from Oak Ridge National Laboratory (ORNL) for their help in providing global ERA5 hourly reanalysis dataset. This research is supported by the Office of Science of the U.S. Department of Energy (DOE) Biological and Environmental Research as part of the Regional and Global Model Analysis program area. Part of this work was completed using Stampede2 supercomputers from Texas Advanced Computing Center (TACC) and Perlmutter supercomputer from National Energy Research Scientific Computing (NERSC). Contact: xzc55@psu.edu, jingyi.hu@psu.edu

**References:**  
Chen, X., Leung, L. R., Feng, Z., & Yang, Q. (2022). Precipitation-moisture coupling over tropical oceans: Sequential roles of shallow, deep, and mesoscale convective systems. *Geophysical Research Letters*, 49.  
Feng, Z., Leung, L. R., Liu, N., Wang, J., Houze, R. A., Li, J., Hardin, J. C., Chen, D., & Guo, J. (2021). A global high-resolution Mesoscale Convective System Database using satellite-derived cloud tops, surface precipitation, and tracking. *Journal of Geophysical Research: Atmospheres*, 126(B).  
Hersbach, H., Bell, B., Bertoldo, P., Hirahara, S., Horanyi, A., Muñoz-Sabater, J., Nicolas, J., Peubey, C., Radu, R., Schepers, D., Simmons, A., Soci, C., Abdalla, S., Abellan, S., Balsamo, G., Bechtold, P., Biavati, G., Bonavita, M., ... Thepaut, J. (2020). The ERA5 global reanalysis. *Quarterly Journal of the Royal Meteorological Society*, 146(720), 1999-2060. <https://doi.org/10.1002/qj.3803>  
Huffman, G. J., Bolvin, D. T., Braithwaite, D., Hu, K.-L., Joyce, R. J., Kidd, C., Nelkin, E. J., Sorooshian, S., Stocker, E. F., Tan, J., Wolf, D. B., & Xie, P. (2020). Integrated multi-satellite retrievals for the Global Precipitation Measurement (GPM) mission (IMERG). *Advances in Global Change Research*, 343-353.  
Mapes, B. E., Warner, T. T., Xu, M., & Negri, A. J. (2003a). Diurnal Patterns of Rainfall in Northwestern South America. Part I: Observations and Context. *Monthly Weather Review*, 131(5), 799-812.  
Mapes, B. E., Warner, T. T., & Xu, M. (2003b). Diurnal Patterns of Rainfall in Northwestern South America. Part III: Diurnal Gravity Waves and Nocturnal Convection Offshore. *Monthly Weather Review*, 131(5), 830-844.  
Yepes, J., Mejia, J. F., Mapes, B., & Poveda, G. (2020). Gravity waves and other mechanisms modulating the diurnal precipitation over one of the rainiest spots on earth: Observations and simulations in 2016. *Monthly Weather Review*, 148(9), 3933-3950.